AFRL-AFOSR-VA-TR-2023-0197

Development of GeSn waveguide lasers for SWIR and MWIR applications

Mathews, Jay
UNIVERSITY OF DAYTON RESEARCH INSTITUTE
230 W 41ST STREET FL 7
NEW YORK, NY,
US

11/22/2022
Final Technical Report

DISTRIBUTION A: Distribution approved for public release.

Air Force Research Laboratory
Air Force Office of Scientific Research
Arlington, Virginia 22203
Air Force Materiel Command

REPORT DOCUMENTATION PAGE

PLEASE DO NOT RETURN YOUR FORM TO THE ABOVE ORGANIZATION.

1. REPORT DATE	**2. REPORT TYPE**	**3. DATES COVERED**	
20221122	Final	**START DATE** 20170201	**END DATE** 20201214

4. TITLE AND SUBTITLE
Development of GeSn waveguide lasers for SWIR and MWIR applications

5a. CONTRACT NUMBER	**5b. GRANT NUMBER**	**5c. PROGRAM ELEMENT NUMBER**
	FA9550-17-1-0146	61102F
5d. PROJECT NUMBER	**5e. TASK NUMBER**	**5f. WORK UNIT NUMBER**

6. AUTHOR(S)
Jay Mathews

7. PERFORMING ORGANIZATION NAME(S) AND ADDRESS(ES)
UNIVERSITY OF DAYTON RESEARCH INSTITUTE
230 W 41ST STREET FL 7
NEW YORK, NY
US

8. PERFORMING ORGANIZATION REPORT NUMBER

9. SPONSORING/MONITORING AGENCY NAME(S) AND ADDRESS(ES)	**10. SPONSOR/MONITOR'S ACRONYM(S)**	**11. SPONSOR/MONITOR'S REPORT NUMBER(S)**
Air Force Office of Scientific Research 875 N. Randolph St. Room 3112 Arlington, VA 22203	AFRL/AFOSR RTB1	AFRL-AFOSR-VA-TR-2023-0197

12. DISTRIBUTION/AVAILABILITY STATEMENT
A Distribution Unlimited: PB Public Release

13. SUPPLEMENTARY NOTES

14. ABSTRACT
Here we report on the final results of the project. While we were not able to achieve the main goal of producing a room temperature GeSn laser, we have made progress toward this goal. We fabricated GeSn waveguides that did not lase at room temperature, but our modeling shows that
we were very near the lasing threshold. Our new model for GeSn waveguide emission can be used as a tool for design of GeSn waveguides, and our results show that lasing should be achievable at room temperature with relatively minor improvements in GeSn quality and device design. We helped validate two new methods for growth of GeSn, both of which could be used to achieve higher quality GeSn materials. We demonstrated a GeSn photodetector with high-speed operation, and our modeling was used to explain the results

15. SUBJECT TERMS

16. SECURITY CLASSIFICATION OF:			**17. LIMITATION OF ABSTRACT**	**18. NUMBER OF PAGES**
a. REPORT	**b. ABSTRACT**	**c. THIS PAGE**	UU	27
U	U	U		

19a. NAME OF RESPONSIBLE PERSON	**19b. PHONE NUMBER** *(Include area code)*
GERNOT POMRENKE	426-8426

DISTRIBUTION A: Distribution approved for public release.

Grant # FA95501710146

Air Force Office of Scientific Research

Program Manager:

Dr. Gernot Pomrenke
Optoelectronics & Photonics
875 North Randolph Street
Suite 325, Room 3112
Arlington, Virginia 22203-1768, USA

Distribution statement: Distribution authorized to US Government Agencies Only

Security classification: Unclassified

Final Report

Time period: 01-Feb-2017 to 14-Mar-2021

Award Number: FA9550-17-1-0146

Submitted by:

Jay Mathews
Associate Professor
Department of Physics
University of Dayton
300 College Park
Dayton, OH 45469-2314
Phone: 937-229-4933
Fax: 937-229-2180
Email: jay.mathews@udayton.edu

DISTRIBUTION A: Distribution approved for public release.

Project summary

Here we report on the final results of the project. While we were not able to achieve the main goal of producing a room temperature GeSn laser, we have made progress toward this goal. We fabricated GeSn waveguides that did not lase at room temperature, but our modeling shows that we were very near the lasing threshold. Our new model for GeSn waveguide emission can be used as a tool for design of GeSn waveguides, and our results show that lasing should be achievable at room temperature with relatively minor improvements in GeSn quality and device design. We helped validate two new methods for growth of GeSn, both of which could be used to achieve higher quality GeSn materials. We demonstrated a GeSn photodetector with high-speed operation, and our modeling was used to explain the results. We

Major results

Amplified spontaneous emission in GeSn waveguides. We have observed amplified spontaneous emission in waveguides made from *n*-type doped GeSn layers grown on Ge-buffered-Si. We have seen this in multiple samples, but we have not observed any lasing. This is due to the interplay between loss and gain in the waveguide cavity. The gain does not overcome the loss, so lasing is not achieved. However, optical gain is achieved, and we do see a nonlinear response in the output power vs. input power. This indicates that we are at the lasing threshold.

Modeling of emission from GeSn waveguides. Based on the observation of amplified spontaneous emission in waveguides made from GeSn, we have developed a numerical model for the emission that incorporates both theoretical and experimental results to reproduce the emission spectrum and power dependence. This model takes into account material properties such as Sn content, strain, doping, temperature, and recombination lifetime, as well as device properties like the waveguide structure and geometry, the mode confinement in the waveguide, interference effects due to variations in index of refraction, and resonant effects due multiple reflections. Although the model was developed based on a particular experiment, we have validated the model by reproducing the results of other GeSn waveguide experiments where lasing was achieved at cryogenic temperatures. This model can be used to predict the output of GeSn waveguides under optical or electrical pumping, and it can be used as a design tool for achieving room temperature lasing in the future.

Photoluminescence from RPCVD grown films. Chip Claflin at AFRL has introduced a new remote plasma-enhanced chemical vapor deposition (RPCVD) technique for growth of high quality Ge and GeSn films. We have observed PL from a number of these films with Sn content up to 6%, including polycrystalline GeSn grown on sapphire substrates. This is the first known PL measured from polycrystalline GeSn. The results indicate that Chip's new method is very promising for producing high-quality GeSn for device applications.

Photoluminescence from II-PLM grown films. Jim Williams at Australia National University (ANU) and Jeff Warrender at US Army ARDEC-Benét Labs (Benét) have developed an alternative method for GeSn fabrication using ion implantation and pulsed laser melting (II-PLM). We measured PL from films with up to 9% Sn, which represents a significant breakthrough considering the material fabrication process is a drastic departure from typical CVD or MBE growth. This

DISTRIBUTION A: Distribution approved for public release.

shows the promise for the II-PLM for fabrication of direct band gap GeSn. Chip Claflin and Jeff Warrender are also now working together to do laser annealing on CVD grown GeSn films.

Modeling of high-speed GeSn photodetectors. We have been working with Josh Hendrickson at AFRL, Greg Sun at UMass-Boston (UMB), and Henry Cheng at National Taiwan University (NTU) on modeling of the spectral response of Ge/GeSn/Ge photodetectors that were fabricated at NTU. The data showed two major anomalies that we have attempted to explain: a peak in the responsivity at 1600 nm and the decrease in responsivity at higher incident power. We built a model for the responsivity spectrum based on the theoretical optical absorption of GeSn, where the structure of the device and its effect on the absorption spectrum are taken into account. Our model reproduces the peak at 1600 nm, which is due to interference effects, and the power dependence is attributed to increased recombination due to Auger and Shockley-Read-Hall effects.

New design for GeSn LED. We designed a new electrically-injected light-emitting device based on Ge/GeSn/Ge quantum wells (QWs). We developed a new low temperature process for deposition of doped poly-Si using co-sputtering of Si and Al, and we had planned to use this to form the *p*-type layer in a *n-i-p* heterostructure diode. We had also hoped to have Chip Claflin's group at AFRL is grow the QW structures for us. Due to equipment and personnel problems, we were not able to move forward with the device fabrication.

Modeling of optical absorption in GeSn materials. We had originally been working with a model developed by myself and José Menéndez at ASU that could predict the optical absorption of GeSn alloys near the direct band gap, but that model did not include any absorption due to the indirect band gap. We have built a new model which incorporates the indirect band gap absorption, yielding a more accurate model that is valid over a larger range of photon energies. Additionally, we are using this model to explore how optical absorption changes in the presence of high background carrier concentration, such as occurs in a light-emitting device. The results indicate that optical gain (negative absorption) can occur in GeSn materials, and the gain increases with increasing Sn content.

Challenges

This project encountered several major obstacles which hindered our performance and ability to achieve the proposed goals. First, obtaining high quality GeSn films was always an issue. The materials provided by ASU tended to be sporadic and of questionable quality, and we were not able to get the Sn concentrations and doping levels we needed. We also obtained materials from John Tolle at ASM, but we were only able to get a few samples, which we used to develop fabrication protocols. We also worked with Chip Claflin at AFRL, who was able to provide some samples, but the inability to introduce doping and the low Sn content that they could achieve severely limited our progress. I also reached out to several other groups, including Jim Kolodzey, but I was not able to get any response from any other growers. Ultimately, without materials with which to produce devices, we were limited in what we could accomplish.

Another major roadblock was the institutional support available here at UD. We do not have a fabrication facility that is available to outside users. Rather, we have a single faculty member (Prof. Andrew Sarangan) who runs his own nanofabrication lab that is critically under-resourced. The

tools were down so much for repair or maintenance that we had trouble accomplishing much in the way of fabrication. Nevertheless, we were able to accomplish some fab work. Unfortunately, that basically stopped with COVID.

Finally, COVID has had a major impact on our ability to make progress. There have been several effects from the COVID situation. First, one of my PhD students, Yining Liu, was in China visiting family and renewing her visa when the COVID crisis started. She was waiting on her visa approval when the US decided to stop processing visas for Chinese citizens. Although we are in the recovery from COVID now, the visa process has not been restarted, so she is still stuck in China. Yining was the student in my group who had been trained on device fabrication, and she was quite proficient by that time. Unfortunately, with her gone I did not have any students with the requisite training to fabricate devices. Second, the nanofabrication lab run by Prof. Sarangan basically shut down due to COVID. Prof. Sarangan became department chair of the Electro-Optics and Photonics department at UD at about the same time, and this has resulted in a lack of maintenance and support in the nanofab. At this time, several tools are down (the ICP-RIE etcher, in particular, which is critical for our device fab) with no foreseeable time for when they will be back up. Third, with social distancing and the university protocols for on-campus research, productivity in the lab is down significantly. All of these things have combined to make research in the COVID era to be a difficult endeavor.

Broader impacts

I have been working in minority outreach for the past few years in an effort to increase participation of African-American and Latinx students in physics and engineering research. As part of this effort, I personally founded and administered a new summer research program at UD, which has now been running for 5 years, and I will be applying for the NSF REU program in August. We have hosted a total of 14 students from underrepresented groups over the summer in the Physics department at UD, with 5 of those students working in my laboratory. Renaud Bruce, who is in the dual-degree engineering program at Morehouse College in Atlanta worked in my lab performing PL measurements under my graduate student Yining Liu. This has resulted in Renaud receiving authorship on the new publication with the II-PLM GeSn, which is a great success for an undergraduate student, particularly one from an underrepresented group. The funding from this project was key to this achievement.

I have also started a new prototype bridge program for underrepresented minority students to establish a path to graduate school and a career in research for students who otherwise would not go to graduate school. This project has provided opportunities for several of these students to get their first experience in research and pave the way for their future careers.

This project has also served as a vehicle for undergraduate research projects for many UD students over the past few years. Many students were able to gain experience in the laboratory and develop critical skills for the workplace, and a very high percentage of the students I have worked with have gone on to graduate school in physics or engineering.

As a result of my work in helping underrepresented minority students, I was awarded the 2019 Diversity and Inclusion Advocacy Recognition prize by The Optical Society (OSA).

DISTRIBUTION A: Distribution approved for public release.

Technical details

Here we present the technical results and analysis of the work performed, broken down by topic.

1. Amplified spontaneous emission in GeSn waveguides

The waveguide structures, schematically shown in Figure 3, were formed using standard CMOS processing techniques. Strip waveguides with width 3 μm and length 4 mm were patterned on the GeSn surface using standard UV contact photolithography. The waveguides were etched using reactive ion etching with BCl_3. The sidewalls were etched down just past the Ge/Si interface. A 180 nm thick layer of SiO_2 was deposited using plasma-enhanced chemical vapor deposition for surface passivation.

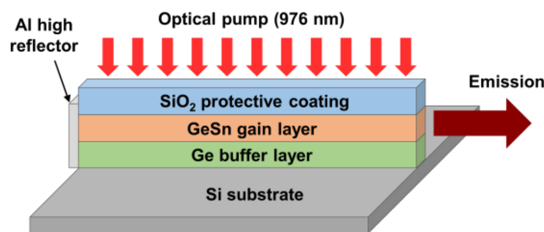

Fig. 3. The GeSn/Ge waveguide structure consisting of the GeSn/Ge stack on Si, SiO_2 coating, and Al high reflector. The waveguide is optically-pumped from the top, and the emission is collected from the uncoated end facet.

The waveguide consists of a GeSn/Ge stack on Si, coated by SiO_2. Since the index of refraction for GeSn is very close to that of Ge, the waveguide will essentially be the entire Ge/GeSn stack. The waveguide heights, which are the sum of the thicknesses of the Ge and GeSn layers for each sample, are presented in Table I. Although the entire GeSn/Ge stack forms the waveguide, only the GeSn region will produce gain. The bottom edge of the waveguide is the Ge/Si interface, due to the large index contrast between Ge and Si. The other three edges of the waveguide cross-section are the Ge/SiO_2 or the GeSn/SiO_2 interface, where there is also a large index contrast. The ends of the waveguide were cleaved to form the end facets, and then they were mechanically polished down to a mirror finish. This resulted in a reduction of the original waveguide length from lithography, and the final lengths are presented in Table I. A 200 nm thick Al film was sputtered onto one facet of each waveguide to form a high reflector (~97% reflection). The Fresnel reflection at the GeSn/Si (36% reflection) serves as the output coupler, where the emission will be collected. A cross-sectional image of the output end of a waveguide from Sample A is shown in Figure 3.

The modes in the waveguide structures were simulated using finite element analysis in COMSOL. These waveguides were determined to be multimode, with 20 or more modes. Figure 4 shows several modes in the waveguide A. In each case, some of the mode is in the active GeSn area, while some of the mode lies in the inactive Ge region. Only the part of the mode in the GeSn area will be subject to gain.

DISTRIBUTION A: Distribution approved for public release.

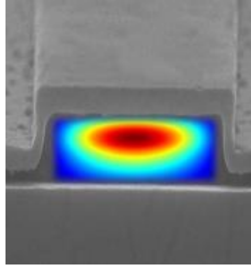

Fig. 4. 2-D intensity plots of the fundamental waveguide mode in sample A found from the finite element analysis using COMSOL. The image is superimposed onto an SEM image of a fabricated waveguide.

The room temperature emission spectra from waveguides with two different Sn concentrations (5.4% and 6.2%) were measured experimentally, and the results are shown in Fig. 2. As expected, the emission peak positions agree with peaks obtained from photoluminescence from the Ge/GeSn stack before waveguide fabrication, which is attributed to band edge emission from the direct band gap. The waveguide emission from Sample A (fig? a) reaches a maximum intensity within the range of 2060 nm – 2090 nm, while the PL (photoluminescence) spectrum showed a peak at 2065 nm (0.60eV). The waveguide emission from Sample B (fig? b) is at a maximum in the range 2100 nm – 2175 nm, and the PL (photo luminescence) shows a peak at 2140 nm (0.58eV). There is likely a small temperature effect due to local heating. The samples are on a temperature-controlled stage, but with the high CW pump levels, there is still some heating of the top surface. The peak positions at higher pump levels from the spectra obtained from both samples appear to red shift due to this local heating (see Discussion).

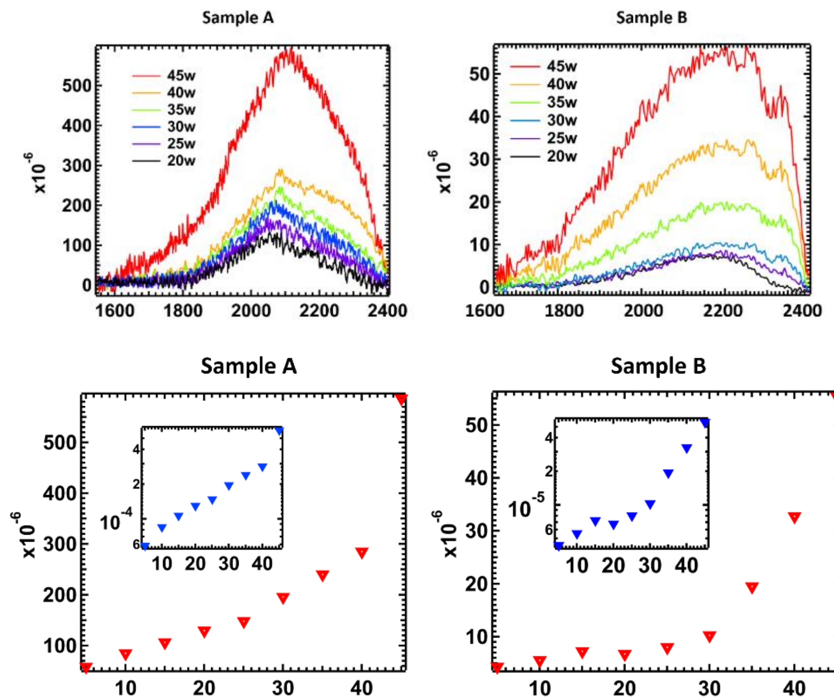

The broadband nature of the waveguide emission demonstrates that lasing has not been achieved. Lasing is characterized by two typical characteristics. One is the narrowing of the emission spectrum as the pump power increases, as spontaneous emission gives way to stimulated emission and the resonant cavity effect increases. The other is a nonlinear dependence of the output power on the pump power, which should have an exponential dependence near the lasing threshold and a linear dependence once lasing is achieved. The spectra shown in Fig. 2 do not show any narrowing of the linewidth, thus the waveguides are not lasing under the conditions in this experiment. However, there could still be some nonlinear dependence in the output power vs. pump power. Fig. 3 shows the integrated area under the spectral curves from Fig. 2 as a function of pump power. The output shows a nonlinear dependence on pump power with a threshold-like behavior. The semi-log plots in the insets show that there is an exponential dependence near the threshold, which would indicate that the waveguides are near the lasing transition. This indicates that there is some optical gain in the waveguides, which is likely due to amplified spontaneous emission or stimulated emission.

An optical active medium is the foundation any laser engineering**.** To understand the physics of our waveguide output power increasing nonlinearly due to higher injection-level indicated a degree of GeSn optical gain at relative spectrum range, we have compared our results with extreme cases; stimulated emission dominated and spontaneous emission dominated spectra-output. Figure X shows the two simple models (scaled to fit) compared with the experimental data for sample B. While the spontaneous emission curve is not perfectly linear, it does not show the threshold behavior that is seen in the experimental data. When compared with the model for stimulated emission, the experimental data does not show as sharp of a threshold as the model. This demonstrates an increasing experimental power curve above pure amplified spontaneous emission (ASE) but still below the case of full stimulated emission, indicating optical gain was provided during the field propagation in terms of photon emission that was partially cost by stimulated radiative recombination. Thus, we developed a model that incorporates both ASE and stimulated emission in order to simulate the emission output spectrum and the total output power as a function of pump power.

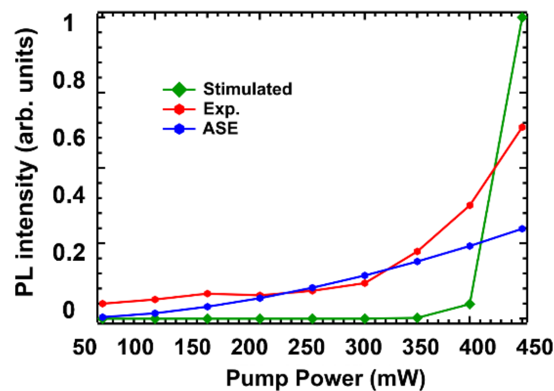

Figure. Plot of experimental output intensity vs. pump power compared with theoretical calculations that include only stimulated emission or amplified spontaneous emission (ASE).

2. Modeling of optical emission from GeSn waveguides

DISTRIBUTION A: Distribution approved for public release.

In order to understand the emission power dependence, we model the waveguide emission in the following way. First, we model the spontaneous emission rate r^{spon} as a function of photon energy $\hbar\omega$ using a generalized Van Roosbroeck-Shockley expression given by

$$r^{spon}(\hbar\omega) = \left(\frac{8\pi n^2\omega^2}{\hbar c^2}\right)\alpha(\hbar\omega)\frac{1}{\exp[\hbar\omega-(E_{Fc}-E_{Fv})]-1}, \quad (1)$$

where n is the index of refraction, E_{Fc} (E_{Fv}) is the quasi-Fermi level for the conduction (valence) bands, $\alpha(\hbar\omega)$ is the absorption coefficient at temperature T, and standard notation is used for physical constants. More details on this model can be found in Ref. (Roucka APL), and the absorption coefficient is modeled as in Ref. (D'Costa PRB). The quasi-Fermi levels for the valence and conductions bands implicitly depend on the excess carrier density, which is determined by the generation of carriers due to absorption of light, i.e. the pump intensity, balanced by the recombination of the carriers. In order to try and model the dependence of the total emission power versus pump intensity, we integrate Eq. 1 over all photon energies for each pump intensity. Relate to the experimental material, the band energy is corrected due to Sn content and material compressive strain introduced during the fabrication process.

Initially, the alloy's unstrained direct band gap E_0with Sn concentration x is calculated using the expression

$$E_0(x) = (1-x)E_0^{Ge} + xE_0^{Sn} - bx(1-x) \qquad 2$$

where $E_0^{Ge} = 0.805eV$ is the unstrained direct band gap of pure Ge, $E_0^{Sn} = -0.4eV$ is the unstrained band gap of α-Sn, and b is the bowing parameter, which is determined from experimental data. In this case the bowing parameter used was b=0.43.[21] The band gap was then corrected for compressive strain using the pseudopotential method. [22]The model for the absorption coefficient near the direct band gap is modeled using the method presented in Roucka et al. [23] The imaginary part of the dielectric function is modeled first using the method in D'Costa et al.,1 except that the contributions from the light and heavy holes are computed separately and combined. The absorption coefficient for empty conduction bands and full valence bands is then calculated as $\alpha_0(E)$. Finally, the absorption coefficient with the bands occupied is approximated by.

$$\alpha(E) = \alpha_0(E)[f_v(E) - f_c(E)]$$

Meanwhile, our detector only captures a fraction of the emitted photons, which is determined by coupling to the detector through the optical system, so we are mainly concerned with the shape of the spontaneous emission power dependence and how it compares to the measured data.

In the simplest case, we assume that the material has a recombination lifetime τ_R, so the excess carrier density Δn is

$$\Delta n = G\tau_R\,, \quad (2)$$

G is the generation rate, which is determined by the pump laser intensity and the absorption coefficient of the GeSn at the pump wavelength. In this case, because the films are highly n-type doped, we assume an effective lifetime of 5 ns. The model for the 4.4% Sn sample is compared to the measured data in Figure 7. While the curve does have some nonlinear dependence, it does not show the threshold-like behavior that is seen in the measured data. We note that adjusting the lifetime between 1 and 10 ns does not change the shape of the spontaneous emission curve.

The lack of coherence and narrowing of the emission spectrum indicate that the emission is not lasing, but the power dependence cannot be explained with spontaneous emission alone. Farther investigation has been done, such that both spontaneous emission of the waveguide and stimulated emission were analyzed. Under a single mode condition, we start off a simple stimulated emission modeling due to material spectrum gain $g(E) = -\alpha(E)$, we have an explanation increasing power spectrum $P(z, E)$ while propagating along the waveguide.

$$\Phi_{\mathrm{stm}} \equiv \frac{\partial P(z, E)}{\partial z} = \Gamma_a g(\omega) P(z, E)$$

For spontaneous emission modeling, the idea of considering propagation spectrum along the waveguides is also applied. Initialized with the assumption of the photon density everywhere in the waveguide is small enough to not cause any significant reduction in the carrier density due to stimulated recombination. Consequently, carrier density spectrum can be calculated as if there were no photons in the waveguide.

$$\Phi_{sp} \equiv \frac{\partial P(z, E)}{\partial z} = \Gamma_a * r_{sp}(E) * \hbar\omega * w * h$$

There for $P(z, E)$ contain stimulated and spontaneous emissions can be presented after considering the total propagation loss a and mirror reflectance at cavity facets.

$$\frac{\partial P(z, \omega)}{\partial z} = \Phi_{\mathrm{sp}} + \Phi_{stm} + (-a + \delta(z - 2L) * \log\left(1 - \frac{1}{R_1 R_2}\right)) P(z, E)$$

However, this function is stiff for modeling the field propagating changes through medium and cavity feedback. We have reformed it into an expansion. First, set:

$$\frac{\partial \Psi(A, B)}{\partial z} = A\Phi_{sp} + B\Phi_{stm} + (-a + \delta(z - 2L) * \log\left(1 - \frac{1}{R_1 R_2}\right)) P(z, E)$$

Solution:

$$P_i(z = 2L, \omega) = \Psi_i(A, B) = B * r_{sp}(\omega) * \hbar\omega * \sigma * \frac{\Gamma_a}{A * \Gamma_a \tilde{g}(\omega) - \tilde{a}} (e^{[A * \Gamma_a \tilde{g} - \tilde{a}]L + \log\left(1 - \frac{1}{R_1 R_2}\right)} - 1)$$

(b.c. P(z=0) =0)

Then:

$$P(z, \omega) = \sum_{i=0}^{m} c_i \Psi_i$$

Since we only care for stimulated and spontaneous emissions as two scenarios, $P(z, \omega)$ can be simplified as:

DISTRIBUTION A: Distribution approved for public release.

$$P_{GeSn}(z,\omega) = c_{sp}\Psi_{sp}(1,0) + c_{stm}\Psi_{stm}(1,1)$$

Physically $\Psi_{sp}(1,0)$ represents the case that all the radiative recombination is spontaneously emitted and $\Psi_{stm}(1,1)$ represents a case of recombination is stimulated by a portion. The reason we chose $\Psi_{stm}(x \neq 0,1)$ instead of $\Psi_{stm}(0,1)$ is that stimulated emission cannot happen without pump. Another practical condition is that the total number of photons output should not exceed the number of excited electron due to pumping. So, we set the limit of photons output as $P_0(z,\omega) = c_o * \Psi_{sp}(1,0)$, where c_l repents the emission power spectrum factor for th round trip. Therefor $c_{sp}$and c_{stm} for the first roundtrip can be rewritten as: ($c_0 = 0.216, from\ experimental\ reslut$)

$$c_{sp} = \frac{c_0}{1+c_0}, c_{stm} = \frac{1}{1+c_0}$$

There for the first round-trip for the emission spectrum can be presented as:

$$P_1(z,\omega) = \frac{c_0}{1+c_0} * \Psi_{sp}(1,0) + \frac{1}{1+c_0} * \Psi_{stm}(1,1)$$

As P_1 is the feedback for the second round-trip, $\widetilde{P_1}(z,\omega)$ is now the reflected power spectrum back into the cavity with the mirror loss $log(\frac{1}{R_1R_2})$:

$$P_2(z,\omega) = \frac{c_1}{1+c_1} * \widetilde{P_1}(z,\omega) + \frac{1}{1+c_1} * \Psi_{stm}(1,1),$$

$where$:

$$\frac{c_1}{c_0} = \frac{\widetilde{P_1}}{P_0},$$

After initial roundtrip, with continues pumping the cavity resonance affect is also needed to apply:

$$P_l(z,\omega) = \frac{c_{l-1}}{1+c_{l-1}} * \widetilde{P_{l-1}}(z,\omega) * cos^2\left(\frac{2\pi z}{n\lambda}\right) + P_0 + \frac{1}{1+c_{l-1}} * \Psi_{stm}(1,1) \qquad \{n \in z, n \geq 2\}$$

Where c(l) keeps checks and balances between the number of excited electrons and total photon emission with continues pumping:

$$\frac{c_{l-1}}{c_{l-2}} = \frac{\widetilde{P_{l-1}}}{P_l + P_0} \qquad \{n \in z, n \geq 2\}$$

Finally, the total emission spectrum with continuous pumping becomes:

$$P_{total}(z,\omega) = P_1(z,\omega) + \sum_{i=2}^{l} P_i \qquad \{l \in Z, l \geq 2\}$$

This model is capable of tracking the field changes at each trip, and we are able to observe the spectrum evolution under certain conditions. As fig? shows in the discussion, we are able to determine at 187th round-trip, the power output only increasing linearly, and waveguide reaches an equilibrium state with spectrum width narrowing stops. Or in fig? we showed that material gain is not large enough for stimulated emission to be built up inside the waveguide and overcome the

cavity threshold, so that increasing of the pump power does not result a width narrowing for any n and c(l) goes to zero.

Since sub 7% Sn content with exile strain does not provide a direct band gap gain medium (need ref.), luminescence from band gap was observed at longer wavelength position. Considering the instrumental broadening, our model reproduced the direct band waveguides emission spectrum. By comparing the differences between direct band emission model with experimental outcome, the band gap emission revives at longer wavelength. It is necessary to point out that in the fig the right-hand 2374.75nm (0.5282eV) peak does not fully represent L band position due to detection limit. The L band energy is lower than 0.5282eV. on the shorter wavelength region of the spectrum and with high pump power, a band at 1998.28nm (0.6205eV) starts to contribute to the emission. (fig?) Since the next two closest band is 0.05eV higher for the ΔE band and 2.42eV higher for the Γ_2 band, it is suggesting a representation of sample B ΔE band at 0.62eV from the plot.

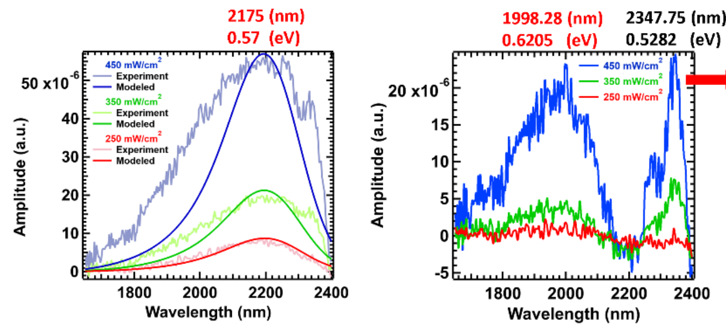

Band energy	Ge	Sample B
Γ (eV)	0.66	0.53eV
L (eV)	0.8	0.57eV
ΔE (eV)	0.85	0.62eV

Initialized by our experimental parameters our model leaded us to understand what improvements of different conditions and parameters are we need, so that field can start to surviving multiple tripes within the cavities and building up the coherence. The success of lasing with high Sn content (ref.) at low temperature gives us opportunities to explore this model outside of our parameters. For an example of the setup from Writh's work, we have simulated their experimental output by using the corresponded Sn content, waveguides structure parameters, pumping conditions, doping

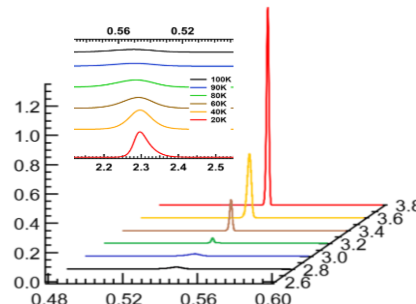

DISTRIBUTION A: Distribution approved for public release.

level and temperature with our model. We predicted lasing at $20K^0$ and spectrum line width narrowing to sub nano meter at 3.8(mW/cm2 ?) (pump level).

With the accurate reproduction of known research, we conducted a series of studies on temperature, injection-level, loss, and carrier lifetime dependences. We are able to predict where lasing would occur due to these dependences changes and how far is our current research away.

First, we consider temperature as the one of the material properties that can control, the direct band emission increases at lower value (ref.). With Sn content level for Sample B 6.2% not high enough to be a direct band material, the portability of phono assist none-radiative transition from L band to the top of valance band will decrease, more active electron will contribute to direct band transition. In such a scenario, material gain is increased. As the fig shows, our model demonstrates a potential lasing condition for Sample B at a lower temperature at 250K with our maximum equipment pump power (45mw/cm2) along with the red shift for spectrum peak due to higher temperature. At 260 K, competitions of the cavity models occur, and the spectrum line width narrows down to sub-nano meter costs spectrum peak amplitude increased dramatically. However lasing at lower temperature is predicted at 50K lower, it does not fulfill the goal of lasing at room temperature.

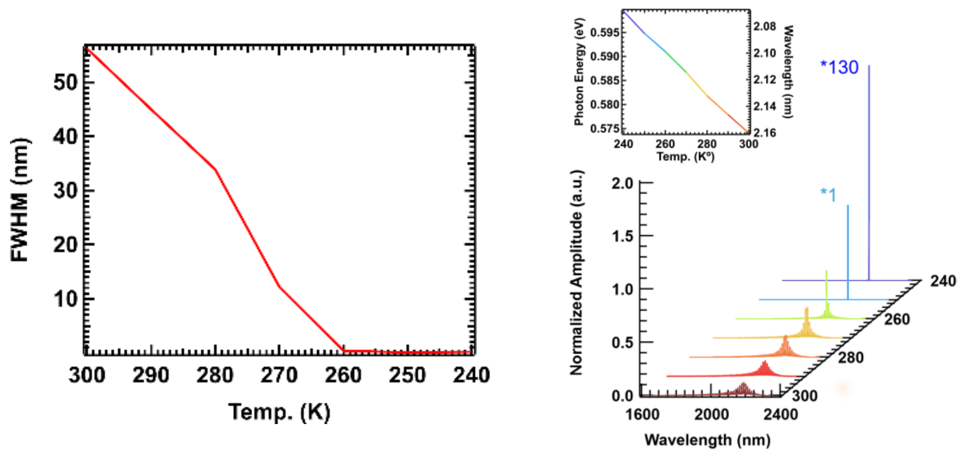

Other than material properties, pumping level and cavity quality are engineering issues. Wavguides surface passivation (ref.) prosses increases the sidewall smoothness lowers the propagation loss of the cavity. On the other hand, instead of rely on Farnell reflection and Al coated facet, a pair of multilayer dielectric coating can be applied to increase the capture of the field

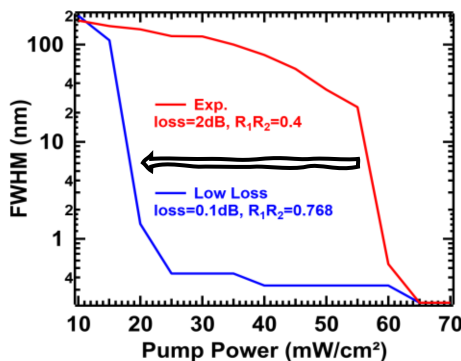

DISTRIBUTION A: Distribution approved for public release.

propagating within the cavity. As fig demonstrates, the red curve represents the modeled line-width changes due to pump power increasing with experimental perimeters fixed, shows spectrum line-width dramatic narrows ~60 mw/cm2 and the blue curve was model with reset experimental parameters except propagation loss changes from 2dB to 0.1 dB and mirror loss changes from 0.4 to 0.768 with dielectric mirror design with a quarter sample B peak wavelength thickness of SiO2 and ZnS. Overall lower cavity loss resulting linewidth narrows at much lower pump level ~ 20mw/cm2 as the potential requirements for stimulated emission overcome the threshold. Unlike changing the material properties, cavity improvements are less fundamental and easier to achieve.

Last, a fabrication improvement in terms of carrier lifetime increases is discussed. as fig shows the red curve demonstrates that with longer carrier lifetime, the required lasing injection-level decreases. Points on the curve were determined in a condition of modeled linewidth narrowing stops and mode competition nearly stop. The modeled spectrum output for 5ns carrier lifetime is at 68.5wm/cm2. For a step size of 0.5mw/cm2 higher, there will be only one mode visible. Other data points were defined as the same. Longer carrier lifetime provides higher gain value, however dPower/dlifetime has an overall deceasing behavior within the discussed region. For the current Sample B crystalline quality in terms of carrier lifetime has sensitive effectiveness within an order of improvements.

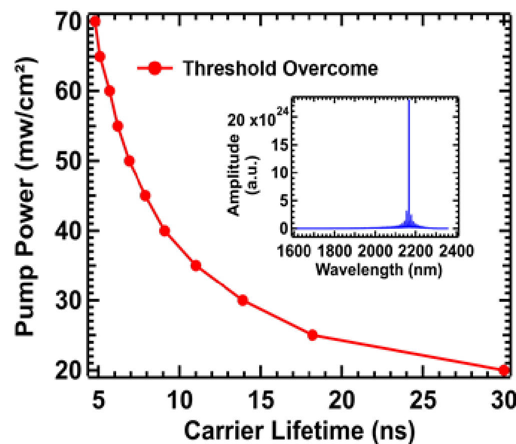

These results indicate that small improvements in GeSn film quality and in the device design should yield room temperature operation for GeSn waveguide lasers.

3. Material synthesis using remote plasma-enhanced chemical vapor deposition

Collaboration with Chip Claflin at AFRL

We have been working closely with Chip Claflin on characterization of GeSn films grown using his new RPCVD method. We have focused on two areas: Measurements of PL emission and defect studies using etch pit density testing.

We have been doing PL measurements for some time, and we have observed room temperature PL from some of the films grown by Chip's group. However, at one point they had to take the reactor apart and rebuild it, and after it was put back together, the material quality seemed to be worse at first. PL emission was not observed in many of the films. However, Chip's group did some tweaking and was able to get it working again. Now, there is an issue with the substrate heater, which is apparently being degraded by the relatively caustic gases being used during the

CVD process and subsequent chamber cleaning. This is limiting the substrate temperature, which is causing issues with growth of the lower Sn content and pure Ge.

Their group is now able to grow the QW structures again, and we are scheduled to get more materials from them in the next month. When we receive the QW structures, we will do PL on them, and then the best samples will be chosen for the LED fabrication.

Another interesting result has been the observation of PL from polycrystalline GeSn. Chip's group has been trying to measure the conductivity of the GeSn films on Si or Ge substrates, but the measurements have proven difficult due to current flowing through the substrate. In order to make an isolated film, they have grown some GeSn on insulating sapphire wafers, forcing the current to stay in the GeSn layer. However, these films are not single crystal materials, as sapphire is not a diamond cubic structure, so the material is polycrystalline.

We performed room temperature PL measurements on one of these samples, and we observed PL signal. This is the first observation of room temperature PL from polycrystalline GeSn, as far as we can tell.

COVID had an impact on this project. Chip's group was not able to produce any materials for some time, but they are back online now. My student, Yining Liu, was the person who did the PL measurements. With her stuck in China, I have been working on training another student to do this work. He is a new grad student, and the training has been slow due to COVID as well. I hope be back to making PL measurements for Chip shortly.

4. Material synthesis using ion implantation and pulsed laser melting
Collaboration with Jim Williams at Australia National University and Jeff Warrender at US Army ARDEC-Benét Labs

We have been working with Jim Williams at ANU and Jeff Warrender at Benét on measuring PL emission from GeSn formed through II-PLM. We started with bulk Ge

Bulk (100) Ge substrates were implanted with Sn ions at an implant energy of $350\ keV$ and implant doses of $4.0-6.8 \cdot 10^{16}\ cm^{-2}$. Prior to the implantation, a $\sim 40\ nm$ capping layer of SiO_2 was deposited on all substrates by plasma-enhanced CVD to prevent Ge from becoming porous. After implantation, the samples were dipped into buffered hydrofluoric acid (HF:NH_4F = 1:7) for $\sim 30\ sec$ to remove the residual SiO_2 capping layer, and $\sim 30\ nm$ of the sample surface was removed by plasma etching (RIE) to get rid of the undesired oxygen before PLM. For the PLM process, a frequency-tripled Nd:YAG laser having a wavelength of $355\ nm$ and a pulse duration of $6\ ns$ was used. The laser fluence was $0.52-0.62\ J \cdot cm^{-2}$

PL measurements were performed on the Ge-Sn alloys using the same setup from Figure 4. The results are shown in Figure 7. PL signal was observed from all three GeSn samples. Fig. 1 shows the normalized PL intensity as a function of wavelength along with the PL signal obtained from a pristine, unimplanted Ge wafer. The peak wavelengths from the GeSn layers are redshifted relative to the unimplanted Ge, as would be expected from the decrease in band gap due to the incorporation of Sn. The width of the peaks from the 5 and $6 \cdot 10^{16}\ cm^{-2}$ samples is much larger than that from the bulk Ge. This is likely due to the gradient in Sn concentration present in the samples rather than the sharp Sn content profile typically obtained using CVD or MBE growth.

The $6.8 \cdot 10^{16}\ cm^{-2}$ sample has a PL peak that is narrower, similar to the bulk Ge, suggesting there is a high-crystallinity region with well-defined Sn content.

The position of the peaks does not correspond with the peak Sn concentrations in the layers. Rather, the PL emission is associated with regions of high-crystallinity. The results indicate that the material in regions with Sn concentration above about 7% is likely somewhat defective. However, production of a high quality region with this Sn content could be used as a basis for further II-PLM to increase the Sn concentration gradually.

Overall, the results indicate that the II-PLM process is a promising candidate for fabrication of GeSn alloys. Further investment into this fabrication process could yield an alternative to epitaxy that avoids many of the complications associated with growth from a template.

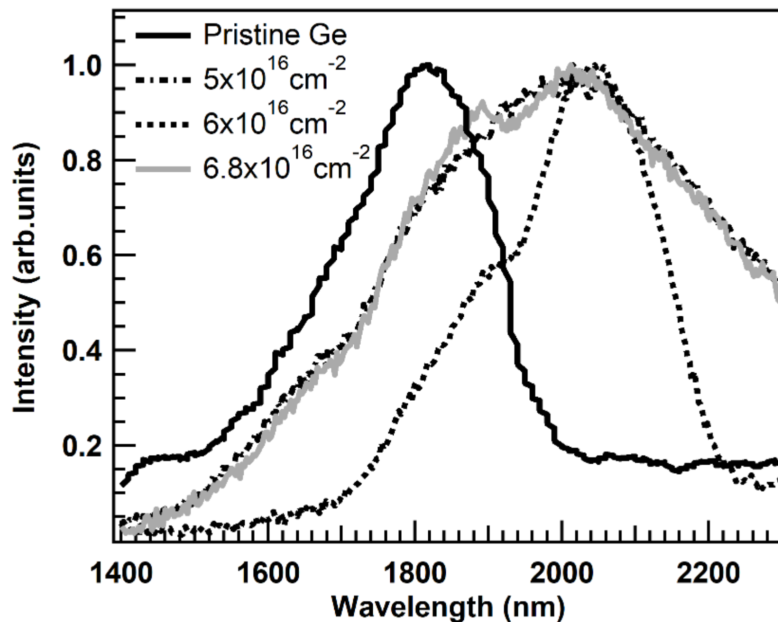

Figure 7. Plot of PL intensity vs. wavelength obtained from GeSn layers fabricated using II-PLM at a variety of implant doses.

One other result of this collaboration is that we have now connected Chip Claflin at AFRL with Jeff Warrender at Benét, and they are now starting a collaboration. The goal is to use the pulsed laser to do laser annealing of the GeSn films grown by Chip to improve the crystallinity. This work is ongoing.

5. Modeling of high-speed photodetectors

Collaboration with Josh Hendrickson at AFRL and Greg Sun at UMass-Boston

We have been working with Josh Hendrickson at AFRL, Greg Sun at UMB, and Henry Cheng at NTU on helping to explain the results of spectral response measurements on Ge/GeSn/Ge heterostructure photodiodes fabricated at NTU and measured at AFRL. I reported on this in my annual report for Y2, but we had some issues with the modeling. We have gone back and done more extensive modeling of the results, including modeling of the index of refraction for the GeSn layer, as well as a more extensive calculation for the amount of light absorbed in the GeSn layer.

Initially, our modeling was based on some assumptions about the index of refraction, and the amount of light absorbed only included a few passes of the light through the GeSn layer.

For the experimental *p-i-n* structure we have developed a model for the external quantum efficiency spectrum over the targeted experimental wavelength range. Starting from a simple model for the EQE in a semi-infinite bulk material we have

$$\mathrm{EQE} = (1-\mathrm{R})\ \eta_c\ (1-\mathrm{e}^{-ad}) \quad , \tag{1}$$

where R is the optical power reflectance at the surface, α is the absorption coefficient at the given wavelength, d is the thickness of the active absorbing layer, and η_c is the fraction of electron-hole pairs that successfully contribute to the detector current, which we term as the collection efficiency. Together $(1-\mathrm{R})$ describes the power that transmitted through the bulk (in our case this will be the thin film layers). The second half $\frac{\int_0^d e^{-ax}dx}{\int_0^\infty e^{-ax}dx} = (1-\mathrm{e}^{-ad})$ describes the absorption weight due to the selected field at the penetration depth (in our case will be the intrinsic layer). In order to account for the thin film structure, we have built our model by modifying the two terms as

$$\mathrm{EQE} = (1-\mathrm{R}-\mathrm{T})\ \eta_c \frac{\mathit{Absorption\ in\ GeSn\ layer}}{\mathit{Total\ Absorption\ in\ the\ structure}}$$

In order to calculate the two absorption components, we look at the electric field distribution in the different regions, which will depend on the propagation through each layer, and integrate the square of the field. We must also account for reflections due to the different indices of refraction in the Ge and GeSn layers. Thus, our expression becomes

$$\mathrm{EQE} = (1-\mathrm{R}-\mathrm{T})\ \eta_c \frac{\int_{d_1}^{d_2} E_{GeSn}^2\, e^{-a_{GeSn}x}dx}{\int_0^{d_1} E_{Ge1}^2\, e^{-a_{Ge}x}dx + \int_{d_1}^{d_2} E_{GeSn}^2\, e^{-a_{GeSn}x}dx}$$

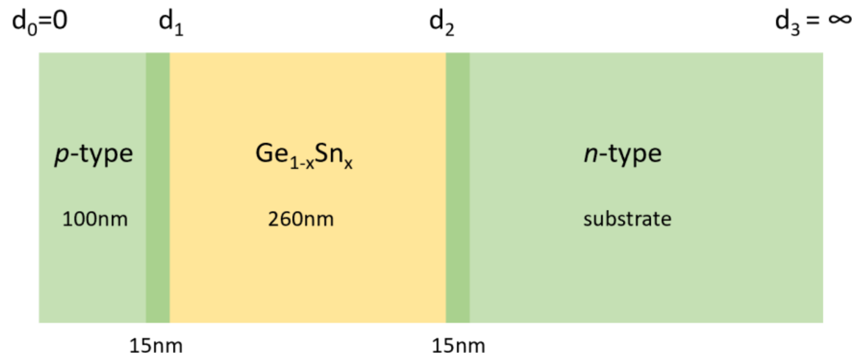

where (1-R-T) represents the absorption of the diode structures, which can be modeled using the transfer matrix method with experimental perimeters from this work, and the distances d_1 and d_2. Fields E_{Ge1}, E_{GeSn} and E_{Ge2} are calculated by summing up all the forward traveling field and backward traveling field , $\boldsymbol{E} = E_n e^{\pm a_n x}$,within each layer that are defined by in between adjacent d_n due to the multiple reflections and transmissions at each interface. Where $E_{Ge1}$is initially normalized as “1”.

To complete the numerical modeling, the optical absorption spectrum and index of refraction (for TMM) are needed for each layer, taking into account the Sn concentration and strain in the layers. Initially, the alloy's unstrained direct band gap E_0 with Sn concentration x is calculated using the expression

$$E_0(x) = (1-x)E_0^{Ge} + xE_0^{Sn} - bx(1-x)$$

where $E_0^{Ge} = 0.805$ eV is the unstrained direct band gap of pure Ge, $E_0^{Sn} = -0.4$ eV is the unstrained band gap of α-Sn, and b is the bowing parameter, which is determined from experimental data. In this case the bowing parameter used was $b = 0.43$. The band gap was then corrected for strain using the pseudopotential method.

The model for the absorption coefficient near the direct band gap is modeled using the method presented in Roucka *et al*. The imaginary part of the dielectric function is modeled first using the method in D'Costa *et al*., except that the contributions from the light and heavy holes are computed separately and combined. The absorption coefficient for empty conduction bands and full valence bands is then calculated as $\alpha_0(E)$. Finally, the absorption coefficient with the bands occupied is approximated by

$$\alpha(E) = \alpha_0(E)[f_v(E) - f_c(E)]$$

where $f_v(E)$ and $f_c(E)$ are the Fermi functions giving the occupation probabilities for the valence and conduction bands, respectively. The absorption length for light in the $Ge_{0.97}Sn_{0.03}$ layer with the measured strain is shown in Fig. A, and the inset shows the absorption coefficient.

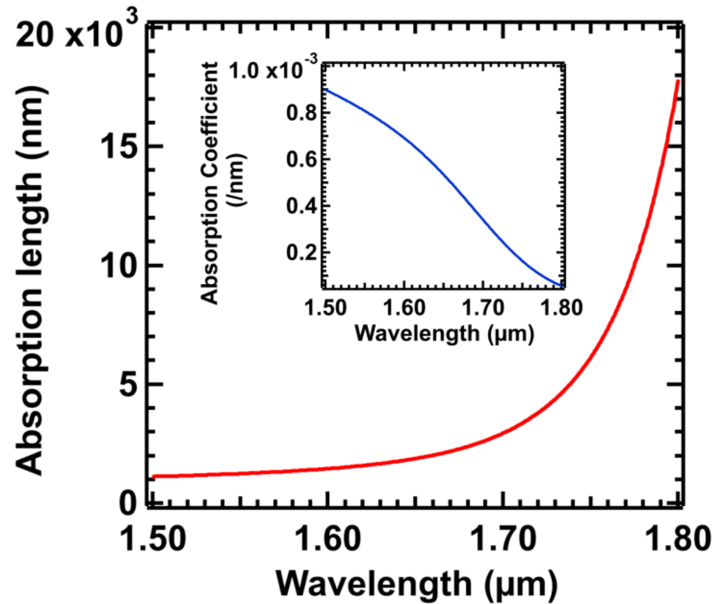

Figure A: Plot of absorption length for $Ge_{0.97}Sn_{0.3}$ layer in nm and its corresponding absorption coefficient.

The wavelength dependence of the index refraction of the layers was modeled using an approximation of the Sellmeier equation

$$n = (D + \frac{E * \lambda^2}{\lambda^2 - F})^{1/2}$$

where D, E, and F are the Sellmeier coefficients. To determine the coefficient values, we used the dependencies found by Tran *et al.*, which give a functional form for the coefficients based on Sn concentration. Since the relaxation of the strain is 95% due to the Ge and $Ge_{0.97}Sn_{0.3}$ interface, the index at each wavelength for the alloy is applied to the modeling is shown below and table I are the material parameters were used to the calculation with the correction due to strain.

D = 15.68,   E = 1.04, F = 1.82

Table I. Sellmeier coefficients used to calculate refractive index of GeSn.

Coefficient	Value
D	15.68
E	1.04
F	1.82

Fig. B shows the wavelength dependence of the indices of refraction of pure Ge and $Ge_{0.97}Sn_{0.03}$ with the measured strain. As we can see the indices of Ge and GeSn do differ enough to make a significant reflection at the interface between them.

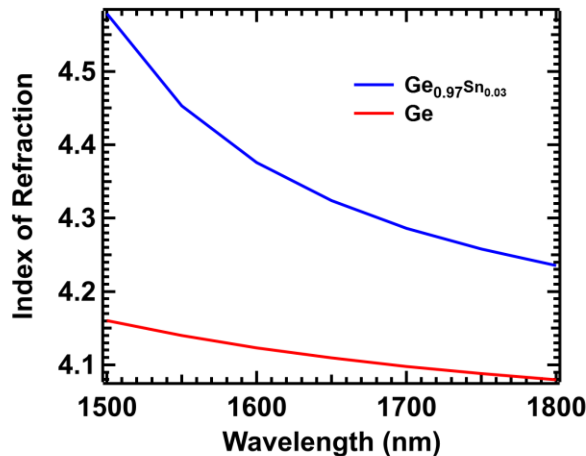

Figure B. Refractive index as a function of wavelength for pure Ge and the $Ge_{0.97}Sn_{0.3}$ layer with the measured strain.

First, we can examine the absorption in the GeSn layer in two cases: as if it was a bulk medium and as a thin layer with our multilayer stack. As shown in Fig. C, the absorption in the layer does change with the addition of the multilayer stack. This is due to the different indices of refraction of GeSn and Ge causing reflection at the interfaces, which serves to narrow the absorption spectrum and decrease the total absorption.

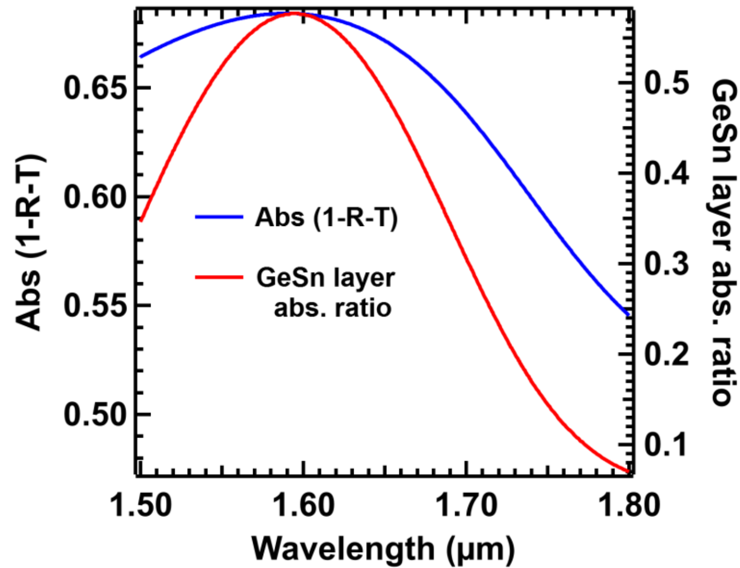

Figure C. Absorption in GeSn layer both with and without multilayer stack.

Now we can compute the EQE spectrum for the device. The collection efficiency η_c is used as a fitting parameter to scale the modeled curve to the experimental data at each power level. Figure D shows the model compared with the experimental data for two different power levels, which result in different collection efficiencies. The model is able to reproduce the peak in the responsivity at 1.6 μm, although the experimental data shows the peak to be somewhat narrower than that produced by the model. The model also agrees well at the longer wavelength (lower energy) edge, but does not agree well on the shorter wavelength (higher energy) edge. These discrepancies are likely due to several factors. First, the model for the absorption coefficient only takes into account the direct band gap absorption, and it agrees well at energies near the band edge. However, as the photon energy deviates from the direct band gap, the approximations starts to underestimate the absorption on the higher energy side.

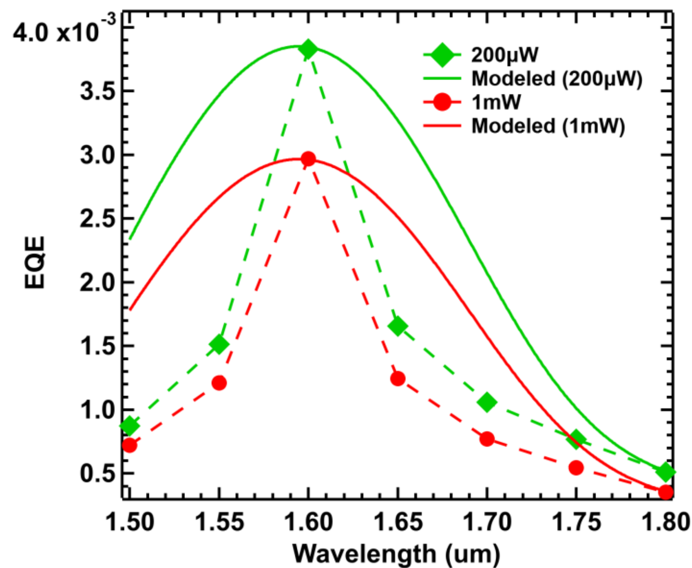

Figure D. Plot of modeled and experimental EQE as a function of wavelength.

The shape of the EQE spectrum does not change much with power, but the overall scaling relative to the model does, which means that the collection efficiency is power dependent. The collection efficiency is dependent on things like the carrier lifetime, the mean travel path of the charge carriers, and the potential differences at the interfaces between the various semiconductor and metal layers. Most of these parameters do not change with power, but the lifetime is affected by power level due to its dependence on the active carrier concentration. As the power level is increased, the injection level increases, thereby decreasing the effective carrier lifetime due to processes such as Shockley-Read-Hall (SRH) and Auger recombination. In Fig. E, we show the dependence of the collection efficiency as a function of power level (which should be roughly proportional to the injection level). As the power level increases, the collection efficiency drops monotonically. For comparison, we show a dependence of the collection efficiency if it were inversely proportional to the square of the power. From this, we see that the collection efficiency is likely inversely proportional to the power to an exponent between 1 and 2.

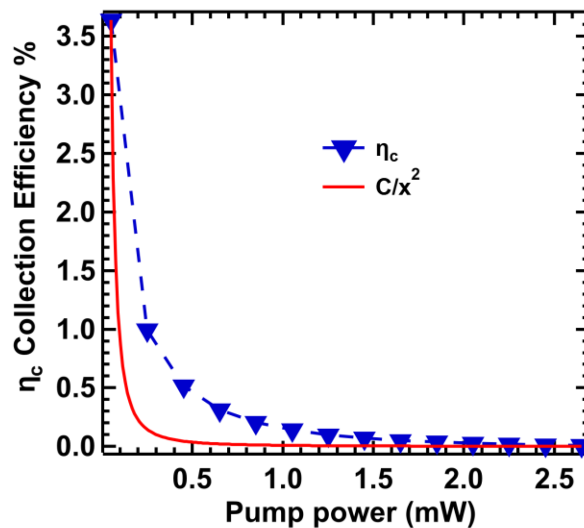

Figure (): modeled collection efficiency spectra plot after fitted to 1600nm experimental responsivity data compared to 1/x^2 where "C" is a fitting constant.

This work should be published soon. The manuscript is currently with our collaborators, and we are waiting on them to move forward.

6. New design for GeSn LED

In my annual report for Y2, I reported on our work with Chip Claflin's group at AFRL, where he was growing GeSn films using a new remote plasma-enhanced chemical vapor deposition technique. This novel method is now producing high-quality GeSn films from which we have measured room temperature photoluminescence. However, there is one capability that Chip's growth system does not have, and that is the ability to dope the GeSn films *in situ* to form *n*-type or *p*-type layers, which is necessary for forming the *p*-*i*-*n* structures around which our waveguide-based laser diodes are based.

This inability to add dopants during growth prompted us to explore new ways to form doped layers after the GeSn growth. We explored several methods, including diffusion doping, ion implantation, and spin-on dopants. However, all of these methods require at least one high temperature annealing step at 600 C or higher. GeSn with Sn content of 2% or higher is not stable at these temperatures, so the annealing will cause segregation or precipitation of Sn. This will cause degradation of the crystalline properties, leading to an increase in nonradiative recombination, thereby dramatically reducing the emission efficiency.

One way to form a *p-i-n* structure is to start with a *n*-type Si wafer, and then grow an intrinsic GeSn layer on top. Once this is done, we can try to deposit some other type of doped layer that is not GeSn to form a heterojunction. We explored a number of different materials using several deposition methods. Ultimately, we found that we could sputter polycrystalline silicon by starting from a highly doped crystalline silicon target. However, even starting with highly doped silicon resulted in a silicon layer with only moderately low resistivity in the 1 Ω-cm range, which is higher than necessary for forming a good contact layer.

In order to decrease the resistivity of the poly-Si, we decided to try co-sputtering with a metal dopant. During the *p*-type silicon sputtering process, we simultaneously sputtered aluminum at a very low power in order to introduce dopant levels of Al, which acts as a *p*-type dopant in Si. Using this method, we are able to achieve resistivities on the order of 0.01 Ω-cm.

Equipped with this new method for formation of heterojunctions, we looked to design an electrically-pumped light-emitting device. Unfortunately, this method will not work for the waveguide designs we came up with previously. Chip's work, however, has taken us in a new direction. His group has been growing Ge/GeSn/Ge quantum well (QW) structures, and we have measured their optical properties. Using this QW approach, we have seen orders of magnitude enhancement in the luminescence power from GeSn. Using only a few nanometers of material in several QWs, we have measured two orders of magnitude more luminescence than in a thick, continuous film of 350 nm. This represents a significant enhancement of the radiative recombination, thereby giving us new hope for achieving optical gain. These new results prompted us to look at a new device design, which I describe below.

The QW structures are very thin layers of GeSn deposited laterally on the wafer. The QW structure provides optical confinement in the vertical direction, thereby enhancing luminescence. Our original waveguide designs are not vertical, however. They are lateral devices with the light propagating horizontally through the waveguide. This means that the QW structures cannot be incorporated into the waveguides, as the enhanced luminescence is vertical, not horizontal. Thus we propose a new device design.

Figure 1 shows a schematic of the device design. We will start with an *n*-type Si wafer, then Chip's group will grow a layer of intrinsic Ge with thickness around 200 nm. Next, they will grow a series of 5-10 nm thick GeSn layers that are sandwiched between Ge layers with thickness >20 nm, ending with Ge. Once that is done, the wafer will be removed from the RPCVD system, and we will bring the wafer to UD, where we will co-sputter the poly-Si and Al to form a *p*++-poly-Si layer with thickness 100 nm. Once the multilayer stack is complete, we will use UV photolithography to define circular mesas and use our GeSn etch recipe to etch the mesas. After

the mesas are formed, we will do another photolithography step to define the contact areas, deposit a metal layer, and then use a lift-off technique to form the contacts.

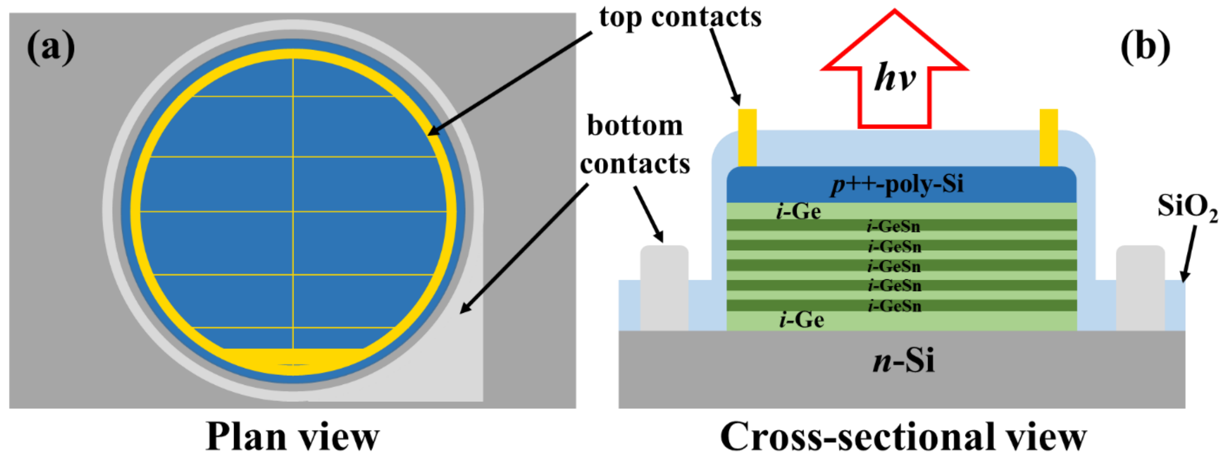

Figure 1. Schematic of device design showing (a) plan view and (b) cross-sectional view of structure.

The device should behave like a diode electrically. When the device is held under forward bias, it should emit light due to electron injection into the conduction band.

Unfortunately, due to COVID, we were not able to fabricate this device. The etching tool in the nanofab, which is key for forming the structure, has been down since just after COVID started. Additionally, my student Yining Liu could not perform the fabrication because she was stuck in China.

7. Modeling of optical absorption in GeSn alloys

We have been working on modeling the optical absorption in GeSn films. The model predicts the absorption coefficient near the band edge, and it takes into account Sn content, strain, temperature, and background carrier concentration.

The model that we had originally been using for the optical absorption in GeSn only included the absorption due to the direct band gap transitions. However, indirect band gap absorption plays a role in absorption in GeSn even near the direct band gap edge, since the indirect and direct band gaps are so close. Thus, we have worked with José Menéndez at ASU to develop a model for the optical absorption that includes the indirect band gap absorption.

The new model works well in reproducing the absorption spectrum for pure, undoped, unstrained Ge, as shown in the figure below.

DISTRIBUTION A: Distribution approved for public release.

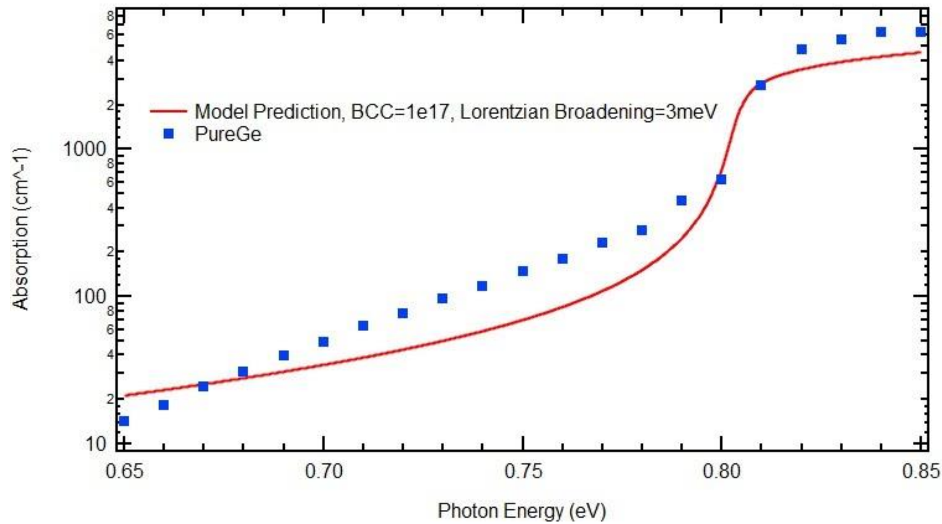

We also used this model to calculate the absorption spectrum for GeSn with 2% Sn and 0.1% tensile strain, which we compare to experimental data obtained via ellipsometry below.

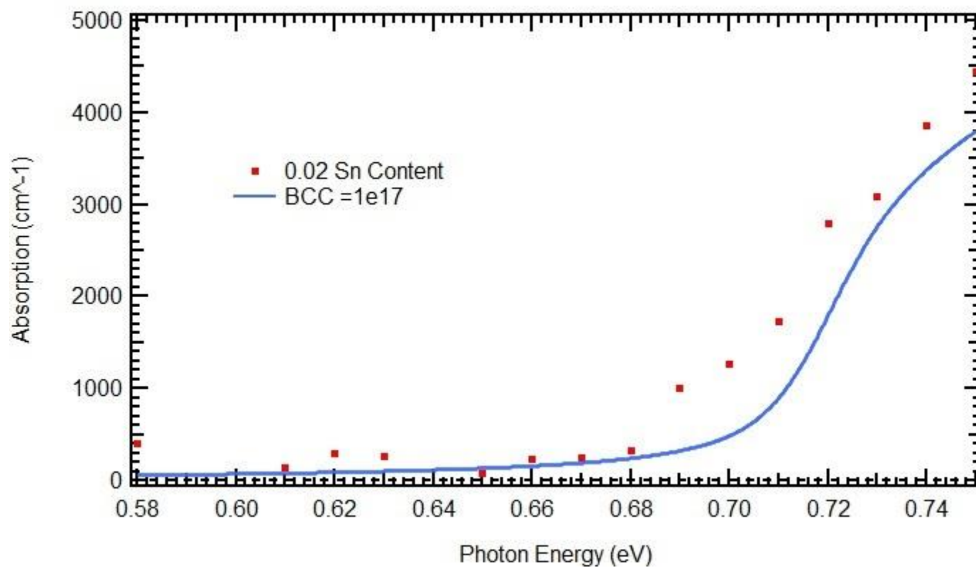

The results for both the pure, unstrained Ge and the GeSn agree well with experiment. Thus, we believe this to be a good model for optical absorption in GeSn.

Much of our theoretical modeling work has been focused on trying to produce GeSn lasers, so we are using this model to explore the behavior of GeSn optically under the type of high injection conditions present in optically- or electrically-pumped devices. We do this by varying the background carrier concentration. For undoped films, this is typically 10^{16} cm^{-3}, and for highly doped films up to about 10^{19} cm^{-3}. In a laser diode or other light-emitting GeSn devices, we expect that the carrier concentrations will go be much higher in the 10^{21} cm^{-3} range.

In the figure below, we show the effect of varying the background carrier concentration. As the background carrier concentration is increased, we see a decrease in optical absorption. At a

background level of 10^{21} cm^{-3}, the absorption near the direct band gap is negative, indicating optical gain.

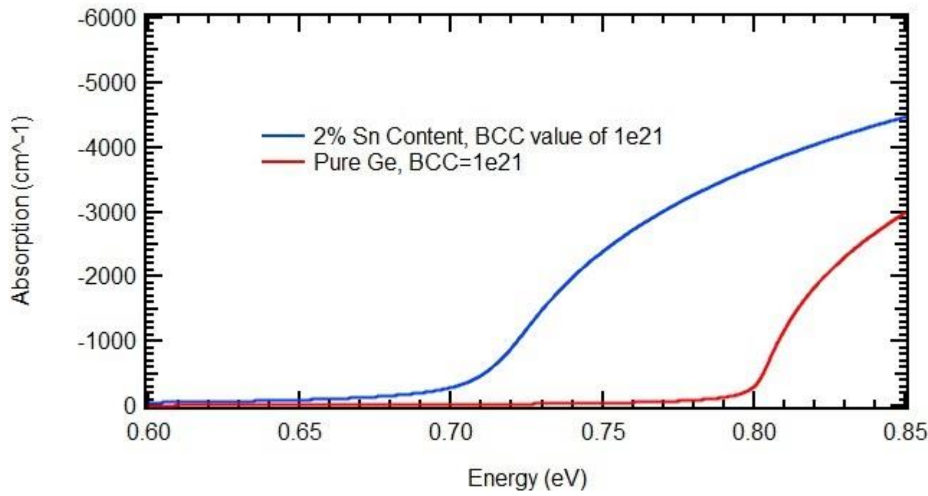

The reason for this negative absorption is the stimulated emission of photons due to the filling of the states in the conduction band. This is not really negative absorption, rather it is that there is more emission than absorption. In other words, we get more light out than we put in due to the presence of the excited charge carriers. This behavior shows up in GeSn, but it even shows up in pure Ge. This helps to explain why lasing has been demonstrated in Ge devices. While the gain is low, the material quality is high, so gain overcomes loss and lasing occurs. The results here also show that more gain is achieved with higher Sn content. However, the trade-off between the increase in gain due to the band structure and the increase in nonradiative recombination due to higher defect densities still present a major challenge for achieving lasing in GeSn devices.

Products

Awards and honors

2019 Diversity and Inclusion Advocacy Recognition Prize, The Optical Society, Jay Mathews, September 11, 2019.

Graduate Student Summer Fellowship, University of Dayton, Yining Liu, April 11, 2019.

Publications

"Synthesis of strain-relaxed Ge-Sn alloys by ion implantation and pulsed laser melting", Tuan T. Tran, Quentin Hudspeth, Buguo Wang, Lachlan A. Smillie, Jay Mathews, Jeffrey M. Warrender, Yung Kee Yeo, J. S. Williams, Mat. Sci. Eng. B 262, 114702 (2020).

"At the lasing threshold: Spontaneous and stimulated emission in GeSn waveguides", Z. Li, Y. Zhao, J. D. Gallagher, D. Lombardo, I. Agha, J. Kouvetakis, J. Menéndez, and J. Mathews, Nature Photonics (in progress).

"Power-dependent investigation of photo-response from GeSn-based p-i-n photodetector operating at high power density," C. Chang, H.-C. Lin, G. Sevison, E. Ghanati, Y. Liu, I. Agha, J. Mathews, R. A. Soref, G. Sun, J. Hendrickson, and H.H. Chen, J. Lightwave Tech. (in progress).

DISTRIBUTION A: Distribution approved for public release.

Presentations

Mathews, J. "Modeling of GeSn waveguide emission." SiGeSn Workshop, Air Force Research Laboratory, Dayton, OH. (September 15, 2020).

Mathews, J. (Presenter & Author), Paper, OSAPS Fall Meeting 2019, Ohio Region Section of American Physical Society, Flint, MI, "GeSn thin film alloys for infrared optoelectronics", Presenter/Lecturer, Academic, Regional, Accepted. (October 12, 2019).

Mathews, J., Tran, T., Liu, Y. (Presenter, graduate student), Hudspeth, Q., Wang, B., Smillie, L., Bruce, R., Warrender, J., and Williams, J. S., Ft. Lauderdale, FL, 2019 IEEE Topical Meeting on Mid-Infrared Optoelectronics in Silicon and Emerging Materials (MOSEM), "Photoluminescence From GeSn Layers Fabricated Using Ion Implantation and Pulsed Laser Melting", Poster, Academic, International, Accepted. (July 9, 2019).

Mathews, J., Invited Lecture or Address, University of West Indies Mona, Kingston, Jamaica, "GeSn alloys for silicon-based optoelectronics", Presenter/Lecturer, Academic, Local, Invited. (June 27, 2019).

Li, Z. (Presenter, graduate student), Gallagher, J., Agha, I., Menéndez, J., Kouvetakis, J., and Mathews, J., Paper, OSAPS Spring Meeting 2019, Ohio Region Section of American Physical Society, Wooster, OH, "Study of On-Si GeSn Gain Spectrum and Amplified Spontaneous Emission", Presenter/Lecturer, Academic, Regional, Accepted. (March 29, 2019).

Ghanati, E. (Presenter, graduate student) and Mathews, J., OSAPS Spring Meeting 2019, Ohio Region Section of American Physical Society, Wooster, OH, "Spontaneous Emission of GeSn via Thin Film Alloys and Quantum Wells", Academic, Regional, Accepted (March 30, 2019).

Mathews, J., Invited Lecture or Address, Morgan State University, Baltimore, MD, "GeSn alloys for silicon-based optoelectronics", Presenter/Lecturer, Academic, Local, Invited. (March 14, 2019).

Scott, C. (Presenter, undergraduate student), Agha, I., and Mathews, J., APS March Meeting 2019, American Physical Society (APS), Boston, MA, " Defect studies in Ge and GeSn thin films grown on Si", Presenter/Lecturer, Academic, International, Accepted. (March 6, 2019).

Mathews, J., Paper, APS March Meeting 2019, American Physical Society (APS), Boston, MA, "Optical spectroscopy of emission from GeSn waveguides on Si", Presenter/Lecturer, Academic, International, Accepted. (March 6, 2019).

Mathews, J. (Presenter & Author), Li, Z., Ghanati, E., Agha, I., Menendez, J., Kouvetakis, J., Paper, AiMES 2018, The Electrochemical Society, Cancun, MX, "Amplified spontaneous emission from GeSn waveguides at room temperature", Presenter/Lecturer, Academic, International, Accepted. (September 30, 2018).

Mathews, J., Invited Lecture or Address, Sensor Directorate (RY), Air Force Research Laboratory, Dayton, OH, "Germanium-tin thin film alloy materials for silicon photonic devices", Academic, Regional, Invited. (June 14, 2018).

DISTRIBUTION A: Distribution approved for public release.

Mathews, J., Invited Lecture or Address, Summer Research Program Weekly Seminar, University of Dayton Physics Department, Dayton, OH, "Germanium-tin thin film alloy materials for silicon photonic devices". (May 24, 2018).

Mathews, J., Invited Lecture or Address, Naval Surface Warfare Center Dahlgren, Fredericksburg, VA, "Advancing silicon photonics: Approaches to producing CMOS-compatible infrared optoelectronics", Presenter/Lecturer, Non-Academic, National, Invited. (May 10, 2018).

Mathews, J., Invited Lecture or Address, Hyperdoping silicon with transition metals for infrared detection, Wright State University Department of Physics, Dayton, OH, Academic, Local, Invited. (February 14, 2018).

Mathews, J. (Presenter & Author), Li, Z. (Author Only), Gallagher, J. (Author Only), Lombardo, D. (Author Only), Agha, I. (Author Only), Menendez, J. (Author Only), Kouvetakis, J. (Author Only), Paper, IEEE Summer Topical Meeting on Mid Infrared Photonics, Institute of Electrical and Electronics Engineers, Waikoloa, HI, "Observation of amplified spontaneous emission in GeSn waveguides at room temperature", Academic, International, Peer-reviewed/refereed, Accepted. (July 9, 2018).

Mathews, J. (Presenter & Author), Li, Z., Ghanati, E., Agha, I., Menendez, J., Kouvetakis, J., Paper, AiMES 2018, The Electrochemical Society, Cancun, MX, "Amplified spontaneous emission from GeSn waveguides at room temperature", Presenter/Lecturer, Academic, International, Accepted. (September 30, 2018).

Mathews, J., Invited Lecture or Address, Sensor Directorate (RY), Air Force Research Laboratory, Dayton, OH, "Germanium-tin thin film alloy materials for silicon photonic devices", Academic, Regional, Invited. (June 14, 2018).

Mathews, J., Invited Lecture or Address, Summer Research Program Weekly Seminar, University of Dayton Physics Department, Dayton, OH, "Germanium-tin thin film alloy materials for silicon photonic devices". (May 24, 2018).

Mathews, J., Invited Lecture or Address, Naval Surface Warfare Center Dahlgren, Fredericksburg, VA, "Advancing silicon photonics: Approaches to producing CMOS-compatible infrared optoelectronics", Presenter/Lecturer, Non-Academic, National, Invited. (May 10, 2018).

Mathews, J., Invited Lecture or Address, Hyperdoping silicon with transition metals for infrared detection, Wright State University Department of Physics, Dayton, OH, Academic, Local, Invited. (February 14, 2018).

Mathews, J. (Presenter & Author), Li, Z. (Author Only), Gallagher, J. (Author Only), Lombardo, D. (Author Only), Agha, I. (Author Only), Menendez, J. (Author Only), Kouvetakis, J. (Author Only), Paper, IEEE Summer Topical Meeting on Mid Infrared Photonics, Institute of Electrical and Electronics Engineers, Waikoloa, HI, "Observation of amplified spontaneous emission in GeSn waveguides at room temperature", Academic, International, Peer-reviewed/refereed, Accepted. (July 9, 2018).

"(Invited) GeSn alloys for Si-based optoelectronics", Howard University, Washington, DC, September 18, 2017.

DISTRIBUTION A: Distribution approved for public release.

"(Invited) Germanium-tin thin film alloy materials for silicon photonic devices",, Second International Workshop on Thin Films for Electronics, Electro-Optics, Energy and Sensors (TFE3S), Institute for Electrical and Electronics Engineers (IEEE), Dayton, OH, June 27, 2017.

Budget expenditures

In the table below, we present the budget expenditures for the full award period compared with the latest budget revision.

Description	Total Spent	Budgeted
Faculty salary	$28,337	$20,289
Graduate student stipends	$120,088	$111,272
Benefits	$30,105	$26,297
Equipment	$54,758	$30,986
Other costs	$34,734	$65,084
Total direct cost	**$268,023**	**$253,928**
Indirect costs	$87,291	$103,668
Total	**$355,314**	**$357,596**

DISTRIBUTION A: Distribution approved for public release.